An Extended Friction Model to capture Load and Temperature effects in Robot Joints

André Carvalho Bittencourt, Erik Wernholt, Shiva Sander-Tavallaey and Torgny Brogårdh

***Abstract*— Friction is the result of complex interactions between contacting surfaces in a nanoscale perspective. Depending on the application, the different models available are more or less suitable. Available static friction models are typically considered to be dependent only on relative speed of interacting surfaces. However, it is known that friction can be affected by other factors than speed.**

In this work, static friction in robot joints is studied with respect to changes in joint angle, load torque and temperature. The effects of these variables are analyzed by means of experiments on a standard industrial robot. Justified by their significance, load torque and temperature are included in an extended static friction model. The proposed model is validated in a wide operating range, reducing the average error a factor of 6 when compared to a standard static friction model.

I. INTRODUCTION

Friction exists in all mechanisms to some extent. It can be defined as the tangential reaction force between two surfaces in contact. It is a nonlinear phenomenon which is physically dependent on contact geometry, topology, properties of the materials, relative velocity, lubricant, etc [1]. Friction has been constantly investigated by researchers due to its importance in several fields [2]. In this paper, friction has been studied based on experiments on an industrial robot.

One reason for the interest in friction of manipulator joints is the need to model friction for control purposes [3]–[7], where a precise friction model can considerably improve the overall performance of a manipulator with respect to accuracy and control stability. Since friction can relate to the wear down process of mechanical systems [8], including robot joints [9], there is also interest in friction modeling for robot condition monitoring and fault detection [9]–[16].

A friction model consistent with real experiments is necessary for successful simulation, design and evaluation. Due to the complexity of friction, it is however often difficult to obtain models that can describe all the empirical observations (see [1] for a comprehensive discussion on friction physics and first principle friction modeling). In a robot joint, the complex interaction of components such as gears, bearings and shafts which are rotating/sliding at different velocities, makes physical modeling difficult. An example of an approach to model friction of complex transmissions can be found in [17], where the author designs joint friction models based on physical models of elementary joint components as helical gear pairs and pre-stressed roller bearings.

Empirically motivated friction models have been successfully used in many applications, including robotics [5], [18]–[20]. This category of models was developed through time according to empirical observations of the phenomenon [2]. Considering a set of states, $\mathcal{X}$, and parameters, θ, these models can be described as the sum of N functions that describe the behavior of friction, $\mathcal{F}$,

$$\mathcal{F}(\mathcal{X}, \theta) = \sum_{i=1}^{N} f_i(\mathcal{X}, \theta). \qquad (\mathcal{M})$$

$\mathcal{X} = [z,\, \dot{q},\, q]$ gives the set of Generalized empirical Friction Model structures (GFM) [1], where z is an internal state related to the dynamic behavior of friction and q is a generalized coordinate and $\dot{q} = dq/dt$.

Among the GFM model structures, the LuGre model [5], [19] is a common choice in the robotics community. For a revolute joint, it can be described as

$$\tau_f = \sigma_0 z + \sigma_1 \dot{z} + h(\dot{\varphi}_m) \qquad (\mathcal{M}_L)$$
$$\dot{z} = \dot{\varphi}_m - \sigma_0 \frac{|\dot{\varphi}_m|}{g(\dot{\varphi}_m)} z,$$

where τ_f is the friction torque and φ_m is the joint motor angle. The state z is related to the dynamic behavior of asperities in the interacting surfaces and can be interpreted as their average deflection, with stiffness σ_0 and damping σ_1. The function $h(\dot{\varphi}_m)$ represents the velocity strengthening (viscous) friction, typically taken as $h(\dot{\varphi}_m) = F_v \dot{\varphi}_m$, and $g(\dot{\varphi}_m)$ captures the velocity weakening of friction. Motivated by the observations of Stribeck [18], [21], $g(\dot{\varphi}_m)$ is usually modeled as

$$g(\dot{\varphi}) = F_c + F_s e^{-\left|\frac{\dot{\varphi}_m}{\dot{\varphi}_s}\right|^{\alpha}}.$$

Where F_c is the Coulomb friction, F_s is, in this paper, defined as the standstill friction parameter*, $\dot{\varphi}_s$ is the Stribeck velocity and α is the exponent of the Stribeck nonlinearity. The model structure $\mathcal{M}_L$ is a GFM with $\mathcal{X} = [z,\, \dot{\varphi}_m]$ and $\theta = [\sigma_0,\, \sigma_1,\, F_c,\, F_s,\, F_v,\, \varphi_s,\, \alpha]$. According to [19] it can successfully describe many of the friction characteristics.

Since z is not measurable, a difficulty with $\mathcal{M}_L$ is the estimation of the dynamic parameters $[\sigma_0,\, \sigma_1]$. In [5], these parameters are estimated in a robot joint by means of open

This work was supported by ABB and the Vinnova Industry Excellence Center LINK-SIC at Linköping University.

A. C. Bittencourt and E. Wernholt are with the Division of Automatic Control, Department of Electrical Engineering, Linköping University, Linköping, Sweden [andrecb,erikw]@isy.liu.se

S. Sander-Tavallaey is with ABB Corporate Research, Västerås, Sweden shiva.sander-tavallaey@se.abb.com

T. Brogårdh is with ABB Robotics, Västerås, Sweden torgny.brogardh@se.abb.com

*F_s is commonly called static friction. An alternative nomenclature was adopted to make a distinction between the dynamic/static friction phenomena.

loop experiments and by use of high resolution encoders. Open-loop experiments are not always possible, and it is common to accept only a static description of $\mathcal{M}_L$. For constant velocities, $\mathcal{M}_L$ is equivalent to the static model $\mathcal{M}_S$:

$$\tau_f(\dot{\varphi}) = g(\dot{\varphi}_m)\text{sign}(\dot{\varphi_m}) + h(\dot{\varphi}_m) \qquad (\mathcal{M}_S)$$

which is fully described by the g- and h functions. In fact, $\mathcal{M}_L$ simply adds dynamics to $\mathcal{M}_S$. The typical choice for g and h as defined for $\mathcal{M}_L$ yields the static model structure $\mathcal{M}_0$:

$$\tau_f(\dot{\varphi_m}) = \left[F_c + F_s e^{-\left|\frac{\dot{\varphi_m}}{\dot{\varphi}_s}\right|^{\alpha}}\right] \text{sign}(\dot{\varphi_m}) + F_v \dot{\varphi_m}. \quad (\mathcal{M}_0)$$

$\mathcal{M}_0$ requires a total of 4† parameters to describe the velocity weakening regime $g(\dot{\varphi}_m)$ and 1 parameter to capture viscous friction $h(\dot{\varphi}_m)$. See Figure 3 for an interpretation of the parameters.

From empirical observations, it is known that friction can be affected by several factors,

- temperature,
- force/torque levels,
- position,
- velocity,
- acceleration,
- lubricant/grease properties.

A shortcoming of the LuGre model structure, as with any GFM, is the dependence only of the states $\mathcal{X} = [z,\, \dot{q},\, q]$. In more demanding applications, the effects of the remaining variables can not be neglected. For instance in [17], the author observes a strong temperature dependence, while in [5] joint load torque and temperature are considered as disturbances and estimated in an adaptive framework. In [9], the influence of both joint load torque and temperature are observed. However, more work is needed in order to understand the influence of different factors on the friction properties. A more comprehensive friction model is needed to improve the performance of control and diagnosis of systems including friction phenomena.

The objective of this contribution is to *analyze and model the effects in static friction related to joint angle, load torques and temperature*. The phenomena are observed in joint 2 of an ABB IRB 6620 industrial robot, see Figure 1(a). Two load torque components are examined, the torque aligned to the joint DoF (degree of freedom) and the torque perpendicular to the joint DoF. These torques are in the paper named manipulation torque τ_m and perpendicular torque τ_p, see Figure 1(b).

By means of experiments, these variables are analyzed and modeled based on the empirical observations. The task of modeling is to find a suitable model structure according to:

$$\tau_f(\mathcal{X}^*, \theta) = \sum_{i=1}^{N} f_i(\mathcal{X}^*, \theta) \qquad (\mathcal{M}^*)$$
$$\mathcal{X}^* = [\dot{\varphi}_m,\, \varphi_a,\, \tau_p,\, \tau_m,\, T]\,,$$

†Many times α is considered a constant between 0.5 and 2 [19].

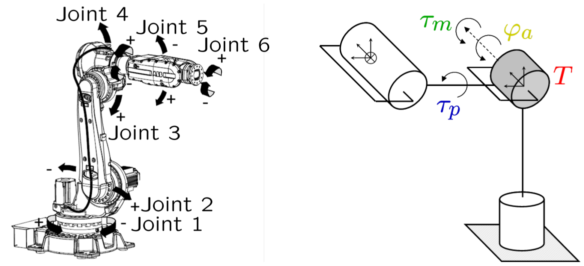

(a) ABB IRB 6620 robot with 150 kg payload and 2.2 m reach.

(b) Schematics of the 3 first joints including the torque definitions for joint 2.

Fig. 1. The experiments were made on joint 2 of the ABB robot IRB 6620. φ_a is the joint angle, T the joint temperature, τ_m the manipulation torque and τ_p the perpendicular torque.

where T is the joint (more precisely, lubricant) temperature and φ_a the joint angle at arm side.

Ideally, the chosen model should be coherent with the empirical observations and, simultaneously, with the lowest dimension of θ, the parameter vector, and with the lowest number of describing functions (minimum N). For practical purposes, the choice of f_i should also be suitable for a useful identification procedure.

The document is organized as follows. Section II presents the method used to estimate static friction in a robot joint, together with the guidelines used during the experiments. Section III contains the major contribution of this work, with the empirical analysis, modeling and validation. Conclusions and future work are presented in Section IV.

II. STATIC FRICTION ESTIMATION AND EXPERIMENTATION

A manipulator is a multivariable, nonlinear system that can be described in a general manner through the rigid body dynamic model

$$M(\varphi_a)\ddot{\varphi}_a + C(\varphi_a, \dot{\varphi}_a) + \tau_g(\varphi_a) + \tau_f = u \qquad (1)$$

where φ_a and φ_m‡ are the vectors of robot angles at arm and motor side of the joint gearbox, $M(\varphi_a)$ is the inertia matrix, $C(\varphi_a, \dot{\varphi}_a)$ relates to speed dependent terms (e.g. Coriolis and centrifugal), $\tau_g(\varphi_a)$ are the gravity-induced torques and τ_f contain the joint friction components. The system is controlled through the input torque, u, applied to the joint motor (in the experiments the torque reference from the servo was measured§).

For single joint movements $(C(\varphi_a, \dot{\varphi}_a) = 0)$ at constant speed $(\ddot{\varphi}_a \approx 0)$, Equation (1) simplifies to

$$\tau_g(\varphi_a) + \tau_f = u. \qquad (2)$$

‡Notice that for the rigid model (1) follows the equivalence $\varphi_a = r \cdot \varphi_m$, where r is the gearbox ratio. Both nomenclatures are kept to emphasize friction as a joint phenomenon.

§It is known that this abstraction might not always hold, for instance under high temperatures. The deviations are however expected to be small and therefore neglected during the experiments.

The applied torque u drives only friction and gravity-induced torques. If realistic estimates of $\tau_g(\varphi_a)$ are available, it is easy to isolate the friction component in Equation (2). If such estimate is not possible (e.g. not all masses are completely known), τ_f can still be estimated as follows.

The required torques to drive a joint in forward, u^+, and reverse, u^-, directions at constant speed $\bar{\dot{\varphi}}_m$ and at a joint angle $\bar{\varphi}_a$ (so that $\tau_g(\varphi_a)$ is equal in both directions), are

$$\tau_f(\bar{\dot{\varphi}}_m) + \tau_g(\bar{\varphi}_a) = u^+$$
$$\tau_f(-\bar{\dot{\varphi}}_m) + \tau_g(\bar{\varphi}_a) = u^-.$$

Subtracting the equations yields

$$\tau_f(\bar{\dot{\varphi}}_m) - \tau_f(-\bar{\dot{\varphi}}_m) = u^+ - u^-$$

and supposing a direction independent friction, i.e. $\tau_f(-\bar{\dot{\varphi}}_m) = -\tau_f(\bar{\dot{\varphi}}_m)$, the resulting direction independent friction is:

$$\tau_f(\bar{\dot{\varphi}}_m) = \frac{u^+ - u^-}{2}. \tag{3}$$

Due to nonlinearities of friction, it is important to define an excitation signal including several different (constant) velocities. The signal used moves *one axis at a time at* 12 *speed levels in both directions*, taking 2:15 min and sampled at 2 KHz¶. Figure 2 shows the motor speed- and torque‖ signals in the experiments.

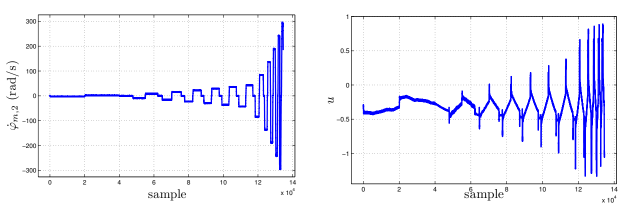

(a) Motor speed (b) Motor applied torque

Fig. 2. Excitation signal used for the static friction curve estimation.

The data was segmented at the different constant speeds and, using Equation (3), the friction torque was computed for each speed. The result of the estimation can then be presented in a *static friction curve*, sometimes referred to as Stribeck curve, see Figure 3. Notice that, since it is assumed that friction is independent of the joint direction of movement, the friction torques for negative velocities would have the same amplitude as in Figure 3 but with opposite sign.

A. Parametric Description and Identification

The solid line in Figure 3 is obtained by model-based estimates of the friction curve with an instance of the static model structure $\mathcal{M}_0$. Since the parameters $\dot{\varphi}_s$ and α enter $\mathcal{M}_0$ in a nonlinear fashion, nonlinear identification methods

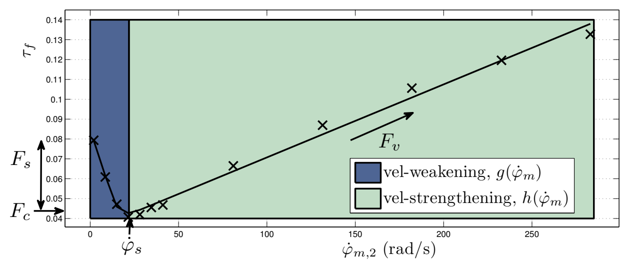

Fig. 3. Static friction values calculated from experiments shown together with $\mathcal{M}_0$ parameters obtained by best fit. The curve is divided into two regions according to its velocity dependent functions, g and h.

are required to achieve their estimate. Considering the static friction curve in the first quadrant, $\mathcal{M}_0$ can be written as the regression

$$\hat{\tau}_f(\dot{\varphi}_m) = f(\dot{\varphi}_m)\theta^T \tag{4a}$$
$$f(\dot{\varphi}_m) = \left[\mathbf{1},\ e^{-\left|\frac{\dot{\varphi}_m}{\dot{\varphi}_s}\right|^{\alpha}},\ \dot{\varphi}_m\right] \tag{4b}$$
$$\theta = [F_c,\ Fs,\ F_v] \tag{4c}$$

where $f(\dot{\varphi}_m)$ is a regressor vector. The chosen identification method combines linear regression with extensive search (grid search over a predetermined range) for the nonlinear parameters $\dot{\varphi}_s$ and α. For the curve in Figure 3, the identified parameters are $[F_c,\ F_s,\ F_v,\ \dot{\varphi}_s,\ \alpha] = [3.40\,10^{-2},\ 4.63\,10^{-2},\ 3.68\,10^{-4},\ 10.70,\ 1.95]$. Notice that, as seen in Figure 3, the model structure $\mathcal{M}_0$ can describe static friction dependence on speed fairly well. In fact, the sum of absolute prediction errors, $\sum|\varepsilon| = \sum|\tau_f - \hat{\tau}_f|$, in Figure 3 is no more than 0.03.

B. Guidelines for the Experiments

In order to be able to build a friction model including more variables than the velocity, it is important to separate their influences. The situation is particularly critical regarding temperature as it is difficult to control it inside a joint. Moreover, due to the complex structure of an industrial robot, changes in joint angle might move the mass center of the robot arm system, causing variations of joint load torques. To avoid undesired effects, the guidelines below were followed during the experiments.

1) Isolating joint load torque dependency from joint angle dependency: Using an accurate dynamic robot model**, it is possible to predict the joint torques for any given robot configuration (a set of all joints angles). For example, Figure 4 shows the resulting τ_m and τ_p at joint 2, related to variations of joint 2 and 4 angles ($\varphi_{a,2}$ and $\varphi_{a,4}$) throughout their workrange. Using this information, a set of configurations *can be selected a priori* in which it is possible to estimate parameters in an efficient way.

2) Isolating temperature effects: Some of the experiments require that the temperature of the joint is under control. Using joint lubricant temperature measurements, the joint thermal decay constant κ was estimated to 3.04 h (see

¶Similar results have been experienced with sampling rates down to 220 Hz.

‖Throughout the paper all torques are normalized to the maximum manipulation torque at low speed.

**An ABB internal tool was used for simulation purposes.

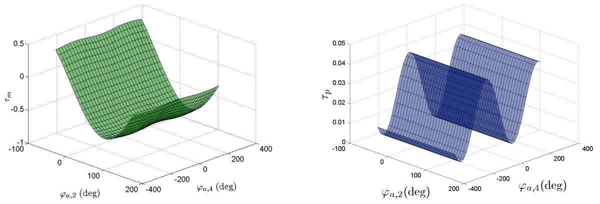

(a) Simulated τ_m (b) Simulated τ_p

Fig. 4. Simulated joint load torques at joint 2. Notice the larger absolute values for τ_m when compared τ_p.

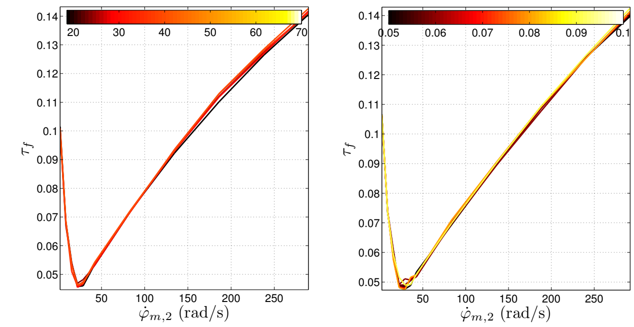

(a) Effects of φ_a at $\tau_m = -0.39$, $T = 34°$ C. (b) Effects of τ_p at $\tau_m = -0.39$, $T = 36°$ C.

Fig. 5. Static friction curves for experiments related to φ_a and τ_p.

[22] for more details). Executing the static friction curve identification experiment periodically, for longer time than 2κ (i.e. $> 6.08\,$h), the joint temperature is expected to have reached an equilibrium. Only data related to the expected thermal equilibrium was considered for the analysis.

III. EMPIRICALLY MOTIVATED MODELING

Using the described static friction curve estimation method, it is possible to design a set of experiments to analyze how the states $\mathcal{X}^*$ affect static friction. As shown in Section II-A, the model structure $\mathcal{M}_0$ can represent static friction dependence on $\dot{\varphi}_m$ fairly well. $\mathcal{M}_0$ is therefore taken as a primary choice, with α considered constant at 1.3 (the value is motivated from [22]). Whenever $\mathcal{M}_0$ can not describe the observed friction behavior, extra terms $f_i(\mathcal{X}^*, \theta)$ are proposed and included in $\mathcal{M}_0$ to achieve a satisfactory model structure $\mathcal{M}^*$.

A. Joint angles

Due to asymmetries in the contact surfaces, it has been observed that the friction of rotating machines depends on the angular position [1]. It is therefore expected that this dependency occurs also in a robot joint. Following the experiment guidelines from the previous section, a total of 50 static friction curves are estimated in the joint angle range $\varphi_a = [8.40,\, 59.00]$deg. As seen in Figure 5(a), little effects can be observed. The subtle deviations are comparable to the errors of the friction curve identified under constant values of $[\varphi_a,\, \tau_p,\, \tau_m,\, T]$. In fact, even a constant instance of $\mathcal{M}_0$ can describe the friction curves satisfactorily, no extra f_i terms are thus required.

B. Joint load torque

Since friction is related to the interaction between contacting surfaces, one of the first phenomena observed was that friction varies according to the applied normal force. The observation is thought to be caused by the increase of the true contact area between the surfaces under larger normal forces. A similar reasoning can be extended to joint torques in a robot revolute joint. Due to the elaborated joint gear- and bearing design it is also expected that torques in different directions will have different effects on the static friction curve††.

††In fact, a full joint load description would require 3 torque and 3 force components.

Because of the mechanical construction of the robot, only small variations of the perpendicular load torque, τ_p, are possible to achieve for joint 2 (see Figure 4(b)). A total of 20 experiments at constant temperature were performed for joint 2, in the range $\tau_p = [0.04,\, 0.10]$. As Figure 5(b) shows, τ_p values in the obtained range did not play a significant role for the static friction curve. No extra terms are therefore needed for joint 2 and $\mathcal{M}_0$ is considered valid. The observation is true at least over a narrow τ_p interval. In [22], a similar experiment is presented for joint 1, for which a larger range of τ_p is possible. In that case a small change in the velocity-weakening regime could be noticed.

As seen in Figure 4(a), large variations of the manipulation torque τ_m are possible by simply varying the arm configuration. A total of 50 static friction curves were estimated over the range $\tau_m = [-0.73,\, 0.44]$. As seen in Figure 6, the effects appear clearly. Obviously, a single $\mathcal{M}_0$ instance can not describe the observed phenomena. A careful analysis of the effects reveals that the main changes occur in the velocity weakening part of the curve. From Figure 6(c), it is possible to observe a (linear) bias-like (F_c) increase and a (linear) increase of the standstill friction (F_s) with $|\tau_m|$. Furthermore, as seen in Figure 6(b), the Stribeck velocity $\dot{\varphi}_m$ is maintained fairly constant. The observations support an extension of $\mathcal{M}_0$ to

$$\begin{aligned}\tau_f(\dot{\varphi}_m, \tau_m) = {} & \{F_{c,0} + F_{c,\tau_m}|\tau_m|\} + \\ & + \{F_{s,0} + F_{s,\tau_m}|\tau_m|\} e^{-\left|\frac{\dot{\varphi}_m}{\dot{\varphi}_{s,\tau_m}}\right|^{1.3}} + F_v \dot{\varphi}_m. \qquad (\mathcal{M}_1)\end{aligned}$$

In the above equation the parameters are written with subscript $_{\text{-}0}$ or $_{\text{-}\tau_m}$ in order to clarify its origin related $\mathcal{M}_0$ or to the effects of τ_m. Assuming that any phenomenon not related to τ_m is constant and such that the $_{\text{-}0}$ terms can capture them, good estimates of the τ_m-dependent parameters can be achieved. Using an identification procedure similar to the one presented in Section II-A, the model $\mathcal{M}_1$ is identified with the data set from Figure 6. The resulting model parameters describing the dependence on τ_m are shown in Table I.

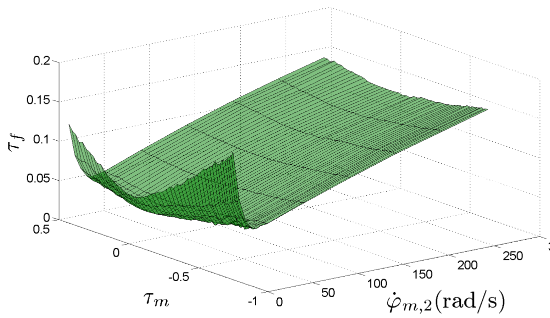

(a) Estimated friction curves for different values of τ_m.

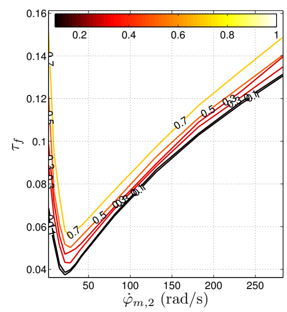

(b) Friction surface cuts for different values of τ_m.

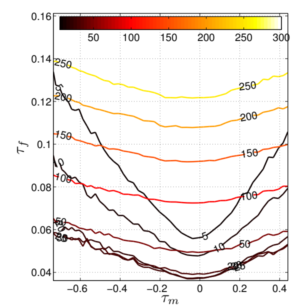

(c) Friction surface cuts for different values of $\dot{\varphi}_{m,2}$ (rad/s).

Fig. 6. The dependence of the static friction curves on the manipulation torque, τ_m, at $T = 34°$ C.

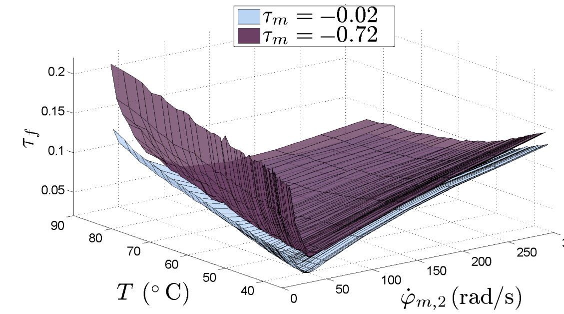

(a) Estimated friction curves for different values of T.

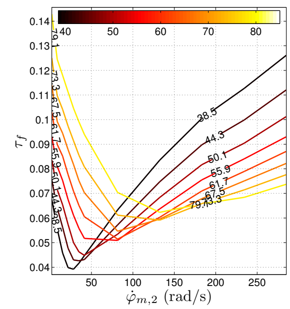

(b) Friction surface cuts for different values of T at $\tau_m = -0.02$.

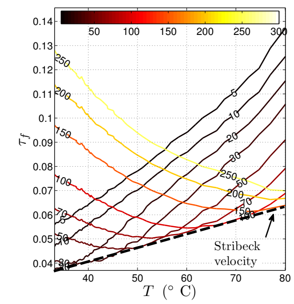

(c) Friction surface cuts for different values of $\dot{\varphi}_{m,2}$ (rad/s) at $\tau_m = -0.02$.

Fig. 7. The temperature dependence of the static friction curve.

TABLE I

IDENTIFIED τ_m-DEPENDENT MODEL PARAMETERS.

F_{c,τ_m}	F_{s,τ_m}	$\dot{\varphi}_{s,\tau_m}$
$2.32\,10^{-2}$	$1.28\,10^{-1}$	9.07

C. Temperature

The friction temperature dependence is related to the change of properties of both lubricant and contacting surfaces. In lubricated mechanisms, both the thickness of the lubricant layer and its viscosity play an important role for the resulting friction properties. In newtonian fluids, the shear forces are directly proportional to the viscosity which, in turn, varies with temperature [23]. Dedicated experiments were made to analyze temperature effects. The joint was at first warmed up to 81.2° C by running the joint continuously back and forth. Then, while the robot cooled, 50 static friction curves were estimated over the range $T = [38.00, 81.20]\,°$ C. In order to resolve combined effects of T and τ_m, two manipulation torque levels were used, $\tau_m = -0.02$, and $\tau_m = -0.72$. As it can be seen in Figure 7, the effects of T are significant.

Temperature has an influence on both velocity regions of the static friction curves. In the velocity-weakening region, a (linear) increase of the standstill friction (F_s) with temperature can be observed according to Figure 7(b). In Figure 7(c) it can moreover be seen that the Stribeck velocity ($\dot{\varphi}_s$) increases (linearly) with temperature. The effects in the velocity-strengthening region appear as a (nonlinear, exponential-like) decrease of the velocity-dependent slope, as seen in Figures 7(b) and 7(c).

It is also interesting to study combined effects of τ_m and T. To better see these effects, the friction surfaces in Figure 7(a) are subtracted from each other, yielding $\tilde{\tau}_f$. As it can be seen from the resulting surface in Figure 8(a), the difference between the surfaces is fairly temperature independent. This is an indication of *independence between effects caused by T and τ_m*.

Given that the effects of T and τ_m are independent, it is possible to subtract the τ_m-effects from the surfaces in Figure 7(a) and solely obtain temperature related phenomena. The previously proposed terms to describe the τ_m-effects in $\mathcal{M}_1$ were:

$$\hat{\tau}_f(\tau_m) = F_{c,\tau_m}|\tau_m| + F_{s,\tau_m}|\tau_m|e^{-\left|\frac{\dot{\varphi}_m}{\dot{\varphi}_{s,\tau_m}}\right|^{1.3}}. \quad (5)$$

With the parameters values given from Table I, the manipulation torque effects were subtracted from the friction curves of the two surfaces in Figure 7(a), that is, the quantities $\tau_f - \hat{\tau}_f(\tau_m)$ were computed. The resulting surfaces are shown in Figure 8(b). As expected, the surfaces become quite similar. The result can also be interpreted as an evidence on the fact that the model structure used for the τ_m-dependent terms and the identified parameter values are correct. Obviously, the original model structure $\mathcal{M}_0$ can not characterize all observed phenomena, even after discounting the τ_m-dependent terms.

A proposal for $\mathcal{M}^*$. From the characteristics of the T-

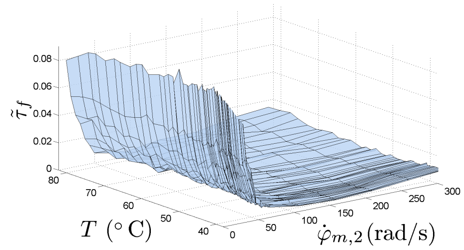

(a) Difference $\tilde{\tau}_f$ between the two static friction surfaces in Figure 7(a).

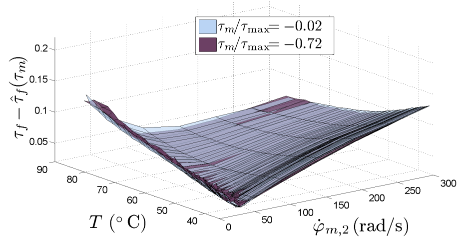

(b) Static friction surfaces in Figure 7(a) after subtraction of the τ_m-dependent terms.

Fig. 8. Indication of independence between effects caused by T and τ_m.

related effects and the already discussed τ_m-effects, $\mathcal{M}_1$ is extended to:

$$
\begin{aligned}
&\tau_f(\dot{\varphi}_m, \tau_m, T) = \\
&\{F_{c,0} + F_{c,\tau_m}|\tau_m|\} + F_{s,\tau_m}|\tau_m| e^{-\left|\frac{\dot{\varphi}_m}{\dot{\varphi}_{s,\tau_m}}\right|^{1.3}} + \quad (\mathcal{M}^*_{g_{\tau_m}}) \\
&+ \{F_{s,0} + F_{s,T}T\} e^{-\left|\frac{\dot{\varphi}_m}{\{\dot{\varphi}_{s,0} + \dot{\varphi}_{s,T}T\}}\right|^{1.3}} + \quad (\mathcal{M}^*_{g_T}) \\
&+ \{F_{v,0} + F_{v,T} e^{\frac{-T}{T_{\mathrm{Vo}}}}\}\dot{\varphi}_m. \quad (\mathcal{M}^*_{h_T})
\end{aligned}
$$

The model describes the effects of τ_m and T for the investigated robot joint. The first $\mathcal{M}^*_g$ expressions relate to the velocity-weakening friction while $\mathcal{M}^*_h$ relates to the velocity-strengthening regime. τ_m only affects the velocity-weakening regime and requires a total of 3 parameters, $[F_{c,\tau_m}, F_{s,\tau_m}, \dot{\varphi}_{s,\tau_m}]$. T affects both regimes and requires 4 parameters, $[F_{s,T}, \dot{\varphi}_{s,T}, F_{v,\tau_m}, T_{\mathrm{Vo}}]$. The 4 remaining parameters, $[F_{c,0}, F_{s,0}, \dot{\varphi}_{s,0}, F_{v,0}]$, relate to the original friction model structure $\mathcal{M}_0$. Notice that under the assumption that τ_m- and T effects are independent, their respective expressions appear as separated sums in $\mathcal{M}^*$.

The term $F_{v,T}e^{-T/T_{\mathrm{Vo}}}$ in $\mathcal{M}^*_{h_T}$ is motivated by the exponential-like behavior of viscous friction (recall Figure 7(c)). In fact, the parameter T_{Vo} is a reference to the Vogel-Fulcher-Tamman exponential description of viscosity and temperature [23].

Given the already identified τ_m-dependent parameters in Table I, the remaining parameters from $\mathcal{M}^*$ are identified from the measurement results presented in Figure 8(b), after the subtraction of the τ_m-terms. The values are shown in Table II.

D. Validation

A separate data set is used for the validation of the proposed model structure $\mathcal{M}^*$. It consists of several static friction curves measured at different τ_m- and T values, as seen in Figure 9. With an instance of $\mathcal{M}^*$ given by

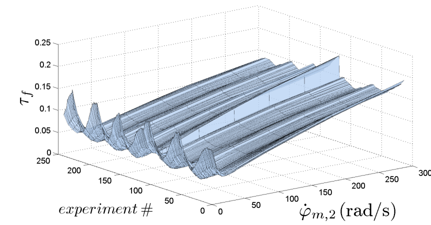

(a) Static friction curves

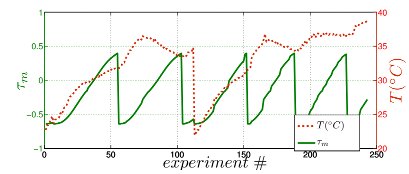

(b) τ_m- and T conditions

Fig. 9. Validation data set. Notice the large variations of T- and τ_m values in Figure (b) when registering the static friction curves in (a).

the parameter values from Tables I and II, the resulting prediction errors for the validation data set are shown in Figure 10. As a comparison, the errors related to a single instance of $\mathcal{M}_0$, with $[F_c, F_s, F_v, \dot{\varphi}_s, \alpha] = [4.90\,10^{-2}, 8.44\,10^{-2}, 5.00\,10^{-4}, 6.50, 1.30]$, are also shown in the figure. As it can be seen, $\mathcal{M}^*$ performs visibly better

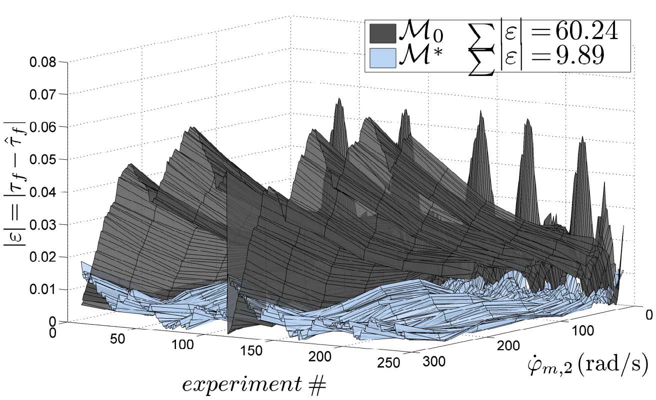

Fig. 10. Models absolute prediction error. Notice the considerable better performance of $\mathcal{M}^*$.

when compared to $\mathcal{M}_0$, with only speed dependence. The maximum and mean errors for $\mathcal{M}^*$ are $[1.86\,10^{-2}, 3.39\,10^{-3}]$, compared to $[7.09\,10^{-2}, 2.07\,10^{-2}]$ for $\mathcal{M}_0$.

IV. CONCLUSIONS AND FURTHER RESEARCH

The main contribution of this paper is the empirically derived model of static friction as a function of the variables $\mathcal{X}^* = [\dot{\varphi}_m, \varphi_a, \tau_p, \tau_m, T]$. While no significant influences of joint angle and perpendicular torque could be found by

TABLE II
IDENTIFIED T-DEPENDENT AND $\mathcal{M}_0$-RELATED MODEL PARAMETERS.

$F_{c,0}$	$F_{c,T}$	$F_{s,0}$	$F_{s,T}$	$F_{v,0}$	$F_{v,T}$	$\dot{\varphi}_{s,0}$	$\dot{\varphi}_{s,T}$	T_{Vo}
$3.04\,10^{-2}$	$4.67\,10^{-6}$	$-2.44\,10^{-2}$	$1.69\,10^{-3}$	$1.29\,10^{-4}$	$1.31\,10^{-3}$	-25.00	1.00	21.00

the experiments, the effects of manipulation torque (τ_m) and temperature (T) were significant. The effects of τ_m and T were included in the proposed model structure $\mathcal{M}^*$, an extended version of the model structure $\mathcal{M}_0$ dependent only on velocity. As shown in Figure 10, the proposed model $\mathcal{M}^*$ is needed in applications where the manipulation torque and the temperature play significant roles.

The description of the velocity-weakening regime, g, in $\mathcal{M}^*$ with an exponential temperature-dependent function was based on the observed phenomena at a (large but) limited temperature range. To capture the static friction behavior at even larger temperature ranges, more complex expressions may be needed [23].

The model $\mathcal{M}^*$ has a total of 7 terms and 3 parameters which enter the model in a nonlinear fashion. The identification of such a model is computationally costly and requires data from several different operating conditions. Studies on defining sound identification excitation and estimation routines are therefore important. It will also be important to validate $\mathcal{M}^*$ on other robot joints and on other robot types and even on other types of rotating mechanisms.

Only static friction (measured when transients caused by velocity changes have disappeared) was considered in the studies. It would be interesting to investigate if a dynamic model, for instance given by the LuGre model structure $\mathcal{M}_L$, could be used to describe dynamic friction with extensions from the proposed $\mathcal{M}^*$. However, to make experiments on a robot joint in order to obtain a dynamic friction model is a big challenge. Probably, such experiments must be made on a robot joint mounted in a test bench instead of on a robot arm system, which has very complex dynamics.

A practical limitation of $\mathcal{M}^*$ is the requirement on availability of τ_m and T. Up to date, torque- and joint temperature sensors are not available in standard industrial robots. The gears of the robot used in the studies was lubricated with oil, not grease, this gave an opportunity to obtain well defined temperature readings by having a temperature sensor in the circulating lubricant oil. Moreover, as mentioned in Section II-B, the joint torque components can still be estimated from the torque reference to the drive system by means of an accurate robot model. In this situation, it is of course important to have correct load parameters in the model in order to calculate the manipulation- and perpendicular torques.

Regardless these experimental challenges, there is a great potential for the use of $\mathcal{M}^*$ for simulation- and evaluation purposes. The designer of control algorithms, the diagnosis engineer, the gearbox manufacturer, etc. would very likely see benefits in using a more realistic friction model.

REFERENCES

[1] F. Al-Bender and J. Swevers, “Characterization of friction force dynamics,” *IEEE Control Systems Magazine*, vol. 28, no. 6, pp. 64–81, 2008.
[2] D. Dowson, *History of Tribology*. Professional Engineering Publishing, London., 1998.
[3] H. M. Kim, S. H. Park, and S. I. Han, “Precise friction control for the nonlinear friction system using the friction state observer and sliding mode control with recurrent fuzzy neural networks,” *Mechatronics*, vol. 19, no. 6, pp. 805 – 815, 2009.
[4] Y. B. Yi Guo, Zhihua Qu, Z. Zhang, and J. Barhen, “Nanotribology and nanoscale friction,” *Control Systems Magazine, IEEE*, vol. 28, no. 6, Dec. 2008.
[5] H. Olsson, K. J. Åström, C. C. de Wit, M. Gafvert, and P. Lischinsky, “Friction models and friction compensation,” *Eur. J. Control*, vol. 4, no. 3, pp. 176–195, 1998.
[6] B. Bona and M. Indri, “Friction compensation in robotics: an overview,” in *Decision and Control, 2005. Proceedings., 44th IEEE International Conference on*, Dec 2005.
[7] F. L. Witono Susanto, Robert Babuska and T. van der Weiden, “Adaptive friction compensation: application to a robotic manipulator,” in *The International Federation of Automatic Control, 2008. Proceedings., 17th World Congress*, Dec 2008.
[8] P. J. Blau, “Embedding wear models into friction models,” *Tribology Letters*, vol. 34, no. 1, Apr. 2009.
[9] A. C. Bittencourt, “Friction change detection in industrial robot arms,” MSc. thesis, The Royal Institute of Technology, 2007.
[10] F. Caccavale, P. Cilibrizzi, F. Pierri, and L. Villani, “Actuators fault diagnosis for robot manipulators with uncertain model,” *Control Engineering Practice*, vol. 17, no. 1, pp. 146 – 157, 2009.
[11] M. Namvar and F. Aghili, “Failure detection and isolation in robotic manipulators using joint torque sensors,” *Robotica*, 2009.
[12] M. McIntyre, W. Dixon, D. Dawson, and I. Walker, “Fault identification for robot manipulators,” *Robotics, IEEE Transactions on*, vol. 21, no. 5, pp. 1028–1034, Oct. 2005.
[13] A. T. Vemuri and M. M. Polycarpou, “A methodology for fault diagnosis in robotic systems using neural networks,” *Robotica*, vol. 22, no. 04, pp. 419–438, 2004.
[14] D. Brambilla, L. Capisani, A. Ferrara, and P. Pisu, “Fault detection for robot manipulators via second-order sliding modes,” *Industrial Electronics, IEEE Transactions on*, vol. 55, no. 11, pp. 3954–3963, Nov. 2008.
[15] R. Mattone and A. D. Luca, “Relaxed fault detection and isolation: An application to a nonlinear case study,” *Automatica*, vol. 42, no. 1, pp. 109 – 116, 2009.
[16] B. Freyermuth, “An approach to model based fault diagnosis of industrial robots,” in *Robotics and Automation, 1991. Proceedings., 1991 IEEE International Conference on*, vol. 2, Apr 1991, pp. 1350–1356.
[17] R. Waiboer, “Dynamic modelling, identification and simulation of industrial robots,” Ph.D. dissertation, University of Twente, 2007.
[18] B. Armstrong-Hélouvry, *Control of Machines with Friction*. Kluwer Academic Publishers, 1991.
[19] K. J. Åström and C. Canudas-de Wit, “Revisiting the lugre friction model,” *Control Systems Magazine, IEEE*, vol. 28, no. 6, pp. 101–114, Dec. 2008.
[20] B. F. S. C. Avraham Harnoy, “Modeling and measuring friction effects,” *Control Systems Magazine, IEEE*, vol. 28, no. 6, Dec. 2008.
[21] R. Stribeck, “Die wesentlichen eigenschaften der gleit-und rollenlager – the key qualities of sliding in roller bearings,” *Zeitschrift Des Vereines Deutcher Ingenieure*, vol. 46, no. 36–38, pp. 1342–1348, 1432–1437, 1902.
[22] A. C. Bittencourt, “Friction in a manipulator joint – an empirical model,” Tech. Report, Linköping University, *to appear*.
[23] C. J. Seeton, “Viscosity-temperature correlation for liquids,” *Tribology Letters*, vol. 22, no. 1, pp. 67–78, Mar. 2006.